DOI 10.1038/n35101998

Crystal structure of the anthrax lethal factor

Andrew D. Pannifer*†, Thiang Yian Wong‡, Robert Schwarzenbacher‡, Martin Renatus‡, Carlo Petosa*†, Jadwiga Bienkowska†§, D. Borden Lacy‖, R. John Collier‖, Sukjoon Park¶, Stephen H. Leppla¶, Philip Hanna# & Robert C. Liddington‡

** Biochemistry Department, University of Leicester, Leicester LE1 7RH, UK*
‡ The Burnham Institute, 10901 North Torrey Pines Road, La Jolla, California 92037, USA
§ Dana Farber Cancer Institute, Boston, Massachusetts 02115, USA
‖ Department of Microbiology and Molecular Genetics, Harvard Medical School, 200 Longwood Avenue, Boston, Massachusetts 02115, USA
¶ National Institute of Dental and Craniofacial Research, National Institutes of Health, 9000 Rockville Pike, Bethesda, Maryland 20892, USA
 # Department of Microbiology and Immunology, University of Michigan Medical School, 5641 Medical Science II, Ann Arbor, Michigan 48109, USA

Lethal factor (LF) is a protein (relative molecular mass 90,000) that is critical in the pathogenesis of anthrax[1–3]. It is a highly specific protease that cleaves members of the mitogen-activated protein kinase kinase (MAPKK) family near to their amino termini, leading to the inhibition of one or more signalling pathways[4–6]. Here we describe the crystal structure of LF and its complex with the N terminus of MAPKK-2. LF comprises four domains: domain I binds the membrane-translocating component of anthrax toxin, the protective antigen (PA); domains II, III and IV together create a long deep groove that holds the 16-residue N-terminal tail of MAPKK-2 before cleavage. Domain II resembles the ADP-ribosylating toxin from *Bacillus cereus*, but the active site has been mutated and recruited to augment substrate recognition. Domain III is inserted into domain II, and seems to have arisen from a repeated duplication of a structural element of domain II. Domain IV is distantly related to the zinc metalloprotease family, and contains the catalytic centre; it also resembles domain I. The structure thus reveals a protein that has evolved through a process of gene duplication, mutation and fusion, into an enzyme with high and unusual specificity.

Anthrax poses a significant threat as an agent of biological warfare and terrorism[7]. Inhalational anthrax, in which spores of *Bacillus anthracis* are inhaled, is almost always fatal, as diagnosis is rarely possible before the disease has progressed to a point where antibiotic treatment is ineffective. The major virulence factors of *B. anthracis* are a poly-D-glutamic acid capsule and anthrax toxin[1]. Anthrax toxin consists of three distinct proteins that act in concert: two enzymes, LF and oedema factor (an adenylate cyclase); and PA. The PA is a four-domain protein[8] that binds a host cell-surface receptor by its carboxy-terminal domain; cleavage of its N-terminal domain by a furin-like protease allows PA to form heptamers that bind the toxic enzymes with high affinity through homologous N-terminal domains. The complex is endocytosed; acidification of the endosome leads to membrane insertion of the PA heptamer by forming a 14-stranded β-barrel[8,9], followed by translocation of the toxic enzymes into the cytosol by an unknown mechanism. The binary combination of PA and LF ('lethal toxin') is sufficient to induce rapid death in animals when given intravenously, and certain metalloprotease inhibitors block the effects of the toxin *in vitro*[10]. Thus, LF is a potential target for therapeutic agents that would inhibit its catalytic activity or block its association with PA.

The MAPKK family of proteins are the only known cellular substrates of LF[4–6]. Cleavage by LF near to their N termini removes the docking sequence for the downstream cognate MAP kinase. The effect of lethal toxin on tumour cells, for example, is to inhibit tumour growth and angiogenesis, most probably by inhibiting the MAPKK-1 and MAPKK-2 pathways[11]. However, the primary cell type affected in anthrax pathogenesis is the macrophage[12,13]. Here, recent evidence shows that low levels of lethal toxin cleave MAPKK-3, inhibiting release, but not production, of the pro-inflammatory mediators, NO and tumour necrosis factor-α (TNF-α)[14]. In contrast, high levels of lethal toxin lead to lysis of macrophages within a few hours, by an unknown mechanism[12]. These observations suggest that at an early stage in infection, lethal toxin may reduce (or delay) the immune response, whereas at a late stage in infection, high titres of the bacterium in the bloodstream trigger macrophage lysis and the sudden release of high levels of NO and TNF-α. This may explain the symptoms before death, which resemble those of septic shock[2].

We solved the structure of LF in two crystal forms with very different packing environments. Nevertheless, differences in tertiary and quaternary structure are small, and the better diffracting crystal form has been refined to 2.2 Å resolution (Figs 1 and 2). The molecule is 100 Å tall and 70 Å wide at its base, with domain I perched on top of the other three domains, which are intimately connected and probably comprise a single folding unit. The only contacts between domain I and the rest of the molecule are with domain II, and these chiefly involve charged polar and water-mediated interactions. The nature of the interface is consistent with the ability of a recombinant N-terminal fragment (residues 1–254) to be expressed as a soluble folded domain that maintains the ability to bind PA and enables the translocation of heterologous fusion proteins into the cytosol[15,16].

Domain I consists of a 12-helix bundle that packs against one face

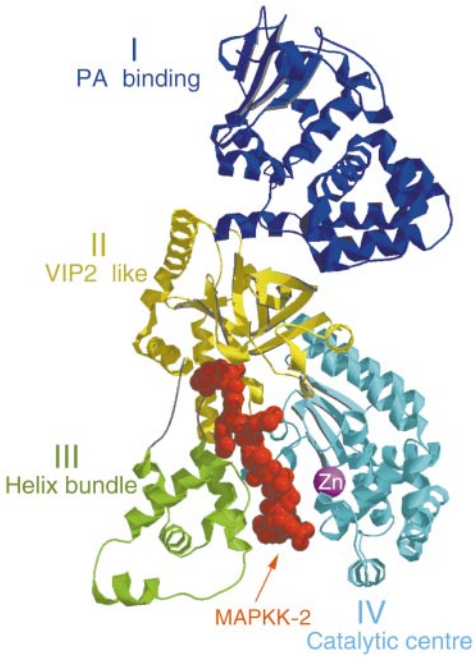

Figure 1 Stereo ribbon representation of LF, coloured by domain. The MAPKK-2 substrate is shown as a red ball-and-stick model, and the Zn^{2+} ion is labelled. The RMSD (Cα) between the cubic and monoclinic crystal forms is 1.18 Å. The principal differences lie in the position of the helical bundle of domain IV, which undergoes a rigid body shift of ~2 Å relative to the β-sheet, and a smaller shift of the β-sheet of domain I. The third helical element of domain III is invisible in the monoclinic crystals, but can be seen in cubic crystals, albeit with high *B*-factors. It is possible that this mobile amphipathic helix has a role in the membrane-inserting properties of LF observed *in vitro*[28]. Figure prepared with MOLSCRIPT, RENDER and RASTER3D[29–31].

† Present addresses: AstraZeneca, Alderley Park, Macclesfield SK10 4TG, UK (A.P.); EMBL Grenoble Outstation, 38042 Grenoble Cedex 9, France (C.P.); Boston University, 36 Cummington Street, Boston, Massachusetts 02215, USA (J.B.).

of a mixed four-stranded β-sheet, with a large (30-residue) ordered loop, L1, between the second and third β-strands forming a flap over the distal face of the sheet. Although there is no detectable sequence homology between domains I and IV, the sheet and two abutting helices can be superposed with a root mean square difference (RMSD) of 2.6 Å. The hallmark metalloprotease motif HExxH is not conserved in domain I; it is replaced by the sequence YEIGK, so Zn^{2+} coordination is not possible. The docking site on domain I for PA is unknown, but the integrity of the folded domain seems to be required, because a series of insertion and point mutants of buried residues in domain I (that presumably disrupt the fold) abrogate binding of PA and toxicity[17,18].

An abrupt turn at the end of the last helix of domain I leads directly into the first helix of domain II (residues 263–297 and 385–550). Although sequence-based comparisons failed to yield any homology, the structural similarity with the catalytic domain of the *B. cereus* toxin, VIP2 (Protein Data Bank accession code 1QS2), is outstanding. Domain II and VIP2 superpose with an RMSD of 3.3 Å and a sequence identity of 15%, as determined by DALI[19]. VIP2 contains an NAD-binding pocket and conserved residues involved in NAD binding and catalysis. Domain II lacks these conserved residues; moreover, a critical glutamic acid that is conserved throughout the family of ADP ribosylating toxins[20] is replaced by a lysine (K518). We therefore expect that domain II does not have ADP-ribosylating activity.

Domain III is a small α-helical bundle with a hydrophobic core (residues 303–382), inserted at a turn between the second and third helices of domain II. Sequence analysis had revealed the presence of a 101-residue segment comprising five tandem repeats (residues 282–382), and suggested that repeats 2–5 arose from a duplication of repeat 1. The crystal structure reveals that repeat 1 actually forms the second helix-turn element of domain II, whereas repeats 2–5 form the four helix-turn elements of the helical bundle, suggesting a mechanism of creating a new protein domain by the repeated replication of a short segment of the parent domain. Domain III is required for LF activity, because insertion mutagenesis and point mutations of buried residues in this domain abrogate function[17]. It makes limited contact with domain II, but shares a hydrophobic surface with domain IV. Its location is such that it severely restricts access to the active site by potential substrates such as the loops of a globular protein; that is, it contributes towards specificity for a flexible 'tail' of a protein substrate. It also contributes sequence specificity by making specific interactions with the substrate (see below).

Domain IV (residues 552–776) consists of a nine-helix bundle packed against a four-stranded β-sheet. Sequence comparisons had failed to detect any homology with other proteins of known structure beyond the HExxH motif. Our three-dimensional structure reveals that the β-sheet and the first six helices can be superposed with those of the metalloprotease thermolysin, with an RMSD of 4.9 Å over 131 residues. Large insertions and deletions occur elsewhere within the loops connecting these elements, so that the overall shapes of the domains are quite different. In particular, a large ordered loop (L2) inserted between strands 4β2 and 4β3 of the sheet partly obscures the active site, packs against domain II, and provides a buttress for domain III.

A zinc ion (Zn^{2+}) is coordinated tetrahedrally by a water molecule and three protein side chains (Fig. 3), in an arrangement typical of the thermolysin family. Two coordinating residues are the histidines from the HExxH motif (His 686 and His 690) lying on one helix (4α4), as expected. Our structure reveals that the third coordinating residue is Glu 735 from helix 4α6. Glu 687 from the HExxH motif lies 3.5 Å from the water molecule, well positioned to act as a general base to activate the zinc-bound water during catalysis. The hydroxyl group of a tyrosine residue (Tyr 728) forms a strong hydrogen bond (O–O distance 2.6 Å) to the water molecule, on the opposite side of Glu 687, and probably functions as a general acid to protonate the amine leaving group.

A broad deep groove, 40 Å long, is contiguous with the active site centre; it is created by the vestigial NAD-binding pocket of domain II and by the interface between domains II, III and IV. The groove has in general a negative potential, containing clusters of glutamic acid/aspartic acid, as well as glutamine/asparagine residues. We introduced peptides corresponding to the N-terminal 16 residues of

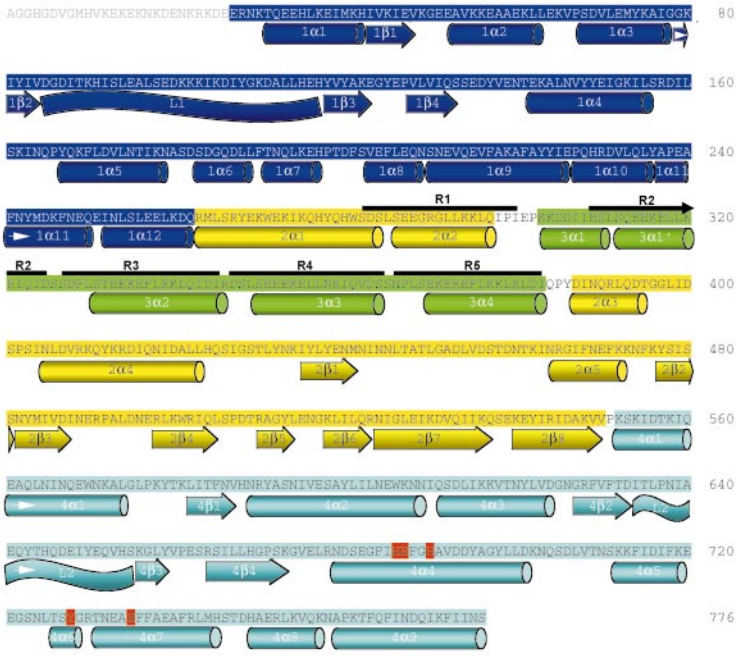

Figure 2 Sequence of LF, coloured as in Fig. 1, with secondary structure indicated. The N-terminal 26 residues are invisible in our electron density maps, and we presume that they are disordered. All other residues are ordered in at least one crystal form. The five sequence repeats are indicated R1–R5. The zinc-coordinating residues are highlighted in red. The sequence of domain I is homologous to the PA-binding domain of oedema factor, and its three-dimensional structure will be similar. For domain II, secondary structure nomenclature matches that of the N-terminal domain of VIP2 (ref. 12).

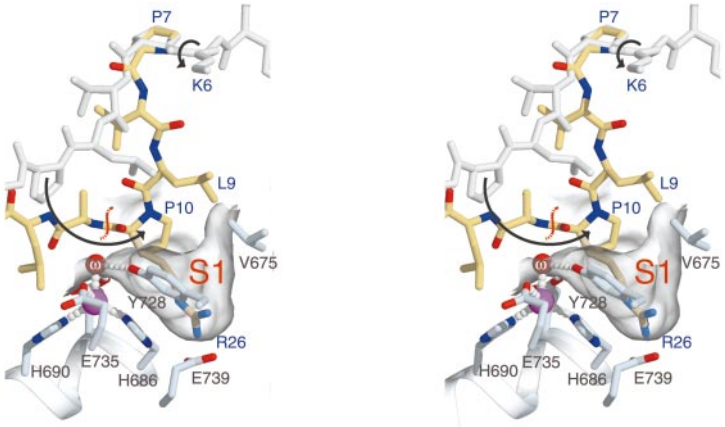

Figure 3 Stereo representation of the active site centre of LF. Zinc-coordinating residues are shown in ball-and-stick representation with the Zn^{2+} ion in magenta and the zinc-bound water labelled ω. Zinc–ligand bond distances are 2.1 ± 0.1 Å (mean ± s.d.). The molecular surface defining the S1 substrate-binding pocket is indicated. Part of the MAPKK-2 model derived crystallographically is shown in grey. A hypothetical model of the productive complex is in yellow, blue and red. A rotation about the Lys 6–Pro 7 main chain would bring Pro 10 into the S1 pocket, positioning the scissile bond close to the zinc-bound water, as indicated. The equivalent residue to Pro 10 in MAPKK-3 is Arg 26, which has a side chain that is also modelled in the S1 pocket, where it could form a salt bridge with the buried Glu 739. A hydrophobic residue (Leu 9 in MAPKK-2) is favoured at the P1′ position, and our model suggests that it can interact with Val 675, at the top of the S1 pocket. Figs 3 and 4 were prepared with SPOCK[32].

MAPKK-2 into crystals of LF. In the absence of Zn^{2+}, we observed continuous electron density that can accommodate the entire 16-residue peptide, extending from domain II through the catalytic centre and ending at the distal end of domain IV (Fig. 4). We observed similar peptide density in the presence of Zn^{2+} in peptide-soaked crystals of a mutant (E687C) that lacks catalytic activity but that binds Zn^{2+} normally[10] (data not shown). A brief (5 min) soak of the wild-type complex in Zn^{2+} led to the disappearance of most of the peptide electron density and a strong peak at the Zn^{2+} position, consistent with activation of the proteolytic machinery. We built a peptide model that shows convincing agreement with the electron density lying in the direction expected for a thermolysin family member. Residues 1–3 sit wholly within the groove of domain II, surrounded by a cluster of asparagine and glutamine residues. Residues 4–10 are sandwiched between domains III and IV. A strongly acidic region of the protein surface rationalizes the preference for basic residues in the MAPKK substrates located 3–6 residues upstream of the cleavage site[6]. Arg 4 makes specific hydrogen bonds with domain III, and Pro 7 points towards an acidic cavity large enough to accommodate the lysine or arginine side chains found in the equivalent positions in MAPKK-1 and -3. Beyond Pro 7, the peptide makes fewer specific contacts.

This is, to our knowledge, the first structural example of a protease in complex with its uncleaved natural substrate. The closest main-chain approach to the Zn^{2+} ion is the scissile bond following Pro 10. However, it is about 6 Å from the zinc-bound water, suggesting that we have captured a 'pre-cleavage' complex. Such complexes have been predicted on the basis of kinetic data[21] but have not previously been observed crystallographically, presumably because, for the shorter recognition sequences of typical proteases, this binding mode is much weaker. Modelling studies show that a rotation about a main-chain dihedral angle at Lys 6 would allow Pro 10 to swing down into the S1 specificity pocket to generate the productive cleavage complex (Fig. 3). This conformational change would not disturb the specific interactions between LF and the N-terminal half of the MAPKK tail. The productive conformation requires an abrupt 90° turn in the peptide chain (favoured by a proline residue) at the P1 position, which would explain why a proline-to-alanine point mutant is not cleaved efficiently[4]. The S1 pocket is very pronounced—hydrophobic at its neck and acidic at its base—appropriate to fit the arginine or lysine side chains found at the P1 position in other MAPKK members[6]. Although the length of the pocket fits the N termini of MAPKK-1 and -2 very well, the pocket is not closed at its N-terminal end, so longer tails, such as those of other MAPKK members, could simply protrude beyond the pocket. At its C terminus, where the globular domain of MAPKK begins, the peptide just protrudes from between domains III and IV. These surfaces may thus provide additional docking sites for other domains on the MAPKK, because fragments of MAPKK-1 lacking the N-terminal tail also bind to LF in a two-hybrid screen[5].

The atomic resolution structure of LF described here demonstrates that the remarkable specificity for MAPKK family members arises in large part from the existence of an extended substrate-binding pocket created by gene duplication and fusion, which recognizes both the structural and sequence properties of its substrate. This information can be used in the design of therapeutic agents that would block the activity of LF *in vivo*. Our structure may also allow the design of mutant LF molecules with altered specificities for different members of the MAPKK family and hence improved anti-tumour properties, for example. □

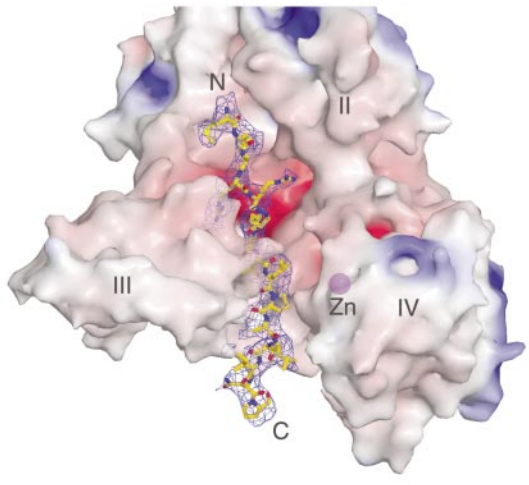

Figure 4 Molecular surface of LF coloured by charge (red, negative; blue, positive), with the model of the MAPKK-2 N-terminal peptide shown in ball-and-stick representation. The electron density surrounding the peptide is a 'simulated annealing omit map' (see Methods) calculated at 3.9 Å resolution and contoured at 0.7σ. Where the model or map would be hidden by the protein surface, the surface is rendered as translucent. A stereo version of this figure is provided in the Supplementary Information.

Methods

Structure of the monoclinic crystal form

LF was purified as described elsewhere[22]. A mixture of cubic and monoclinic crystals were grown from 13 mg ml^{-1} LF, 1.7–1.9 M ammonium sulphate, 0.2 M Tris buffer at pH 7.5–8.0, by the hanging-drop vapour diffusion method. The predominant crystal form is cubic ($I4_132$ a = 331 Å); these crystals diffract to 3.8 Å resolution. Monoclinic crystals ($P2_1$ a = 96.2 Å, b = 137.5 Å, c = 98.6 Å, β = 98.4°) were selectively obtained by macroseeding, and these diffract to 2.2 Å resolution. Derivatives of the monoclinic form were prepared by transferring the crystals to a stabilization buffer containing 2 M lithium sulphate, 200 mM Tris at pH 7.5, and either 50 mM trimethyl-lead acetate for 8 h or 15 mM potassium hexaiodoplatinate for 45 min. Native data were collected on station 9.6 at the Synchrotron Radiation Source (SRS) (Daresbury, UK); a platinum derivative data set was collected on an R-Axis IV image plate, and a multiple (three)-wavelength anomalous diffraction (MAD) data set from the lead derivative was collected on BM14 at the European Synchrotron Radiation Facility (ESRF) (Grenoble). All data were collected at 100 K after transfer to a cryoprotectant containing 25% glycerol. Data were indexed, integrated and scaled with the HKL package[23] and heavy-atom sites were identified and refined with FHSCAL, FFT and MLPHARE from the CCP4 suite[24] or with the program SOLVE[25]. The final figure of merit was 0.51 at 3.2 Å. The rotational component of a two-fold noncrystallographic symmetry (NCS) axis was identified with POLARRFN[24] and the translation with GETAX[24]. Model building was carried out by the graphics program TURBO-FRODO[26] and refined with CNS[27] using all data and a bulk solvent correction. A monomer mask was identified in a map solvent flattened with DM, allowing strict NCS constraints to be used in model building and map calculation. The R-factor converged at around 30%; NCS constraints were released and a further cycle of refinement resulted in a drop in the R_{free} of almost 3%. Multiple cycles of refinement, rebuilding and addition of water molecules reduced the R-factors to final values of 0.225 (R_{work}) and 0.26 (R_{free}) at 2.2 Å. The resulting model fell within, or exceeded, the limits of all the quality criteria of the program PROCHECK[24]. The final model contains 1,497 residues (residues 27–773 of molecule A and 27–776 of molecule B), 934 water molecules, 2 sulphate ions and 2 zinc ions. A table of crystallographic statistics is provided in Supplementary Information.

Structure of the cubic crystal form

We solved cubic structure by molecular replacement with MOLREP[24], using the refined model of the $P2_1$ crystal form converted to polyalanine as a search probe. The cubic crystals contained one molecule in the asymmetric unit and 86% solvent. The initial solution (R_{free} = 0.49) underwent preliminary refinement using rigid body minimization and simulated annealing procedures in CNS[27] to R_{free} = 0.38. Owing to the limited resolution (3.8 Å) and the rapid fall-off in diffraction intensity, the data were sharpened with an overall B-factor of 50 Å^2 (on I), to increase the weight of the high-resolution terms. The resulting difference and omit maps used for rebuilding revealed higher resolution features, such as improved side-chain density.

Structure of peptide complex

The monoclinic crystals cracked on exposure to MAPKK peptides, so the cubic form was used for substrate binding studies. The highest peptide occupancy was achieved with a 5-min room-temperature soak of crystals in 10 mM MAPKK-2 peptide (MLARRKPVLP ALTINP) in cryoprotectant in the absence of zinc. A $2F_o - F_c$ map revealed an additional elongated stretch of electron density in the active site crevice. A peptide model containing the MAPKK-2 sequence was built and subjected to further cycles of refinement and rebuilding with the programs REFMAC5[24] and TURBO-FRODO[26]. Periodically and for final maps, model bias was minimized by excluding the peptide from the phasing and carrying out a cycle of refinement ('simulated annealing omit map'[27]). Assuming an occupancy of 0.7, the peptide main chain B-factors refine to values similar to those of the protein. The final model for the cubic data has been refined to R_{free} = 0.316 (0.402 in the 3.9–4.0 Å shell), R_{work} = 0.295.

Received 16 July; accepted 18 September 2001.

1. Leppla, S. H. in *Comprehensive Sourcebook of Bacterial Protein Toxins* 2nd edn (eds Alouf, J. A. & Freer, J.) 243–263 (Academic, London, 1999).
2. Dixon, T. C., Meselson, M., Guillemin, J. & Hanna, P. C. Medical progress: anthrax. *N. Engl. J. Med.* **341,** 815–862 (1999).
3. Pezard, C., Berche, P. & Mock, M. Contribution of individual toxin components to virulence of *Bacillus anthracis*. *Infect. Immun.* **59,** 3472–3477 (1991).
4. Duesbury, N. S. *et al.* Proteolytic inactivation of MAP-kinase-kinase by anthrax lethal factor. *Science* **280,** 734–737 (1998).
5. Vitale, G. *et al.* Anthrax lethal factor cleaves the N-terminus of MAPKKs and induces tyrosine/threonine phosphorylation of MAPKs in cultured macropahges. *Biochem. Biophys. Res. Comm.* **248,** 706–711 (1998).
6. Vitale, G., Bernardi, L., Napolitani, G., Mock, M. & Montecucco, C. Susceptibility of mitogen-activated protein kinase kinase family members to proteolysis by anthrax lethal factor. *Biochem. J.* **352,** 739–745 (2000).
7. Inglesby, T. V. *et al.* Anthrax as a biological weapon: medical and public health management. Working group on civilian biodefense. *J. Am. Med. Assoc.* **281,** 1735–1745 (1999).
8. Petosa, C., Collier, R. J., Klimpel, K. R., Leppla, S. H. & Liddington, R. C. Crystal structure of the anthrax toxin protective antigen. *Nature* **385,** 833–838 (1997).
9. Benson, E. L., Huynh, P. D., Finkelstein, A. & Collier, R. J. Identification of residues lining the anthrax protective antigen channel. *Biochemistry* **37,** 3941–3948 (1998).
10. Klimpel, K. R., Arora, N. & Leppla, S. H. Anthrax toxin lethal factor contains a zinc metalloprotease consensus sequence which is required for lethal toxin activity. *Mol. Microbiol.* **13,** 1093–1100 (1994).
11. Duesbery, N. S. *et al.* Suppression of ras-mediated transformation and inhibition of tumour growth and angiogenesis by anthrax lethal factor, a proteolytic inhibitor of multiple MEK pathways. *Proc. Natl Acad. Sci. USA* **98,** 4089–4094 (2001).
12. Friedlander, A. M. Macrophages are sensitive to anthrax lethal toxin through an acid-dependent process. *J. Biol. Chem.* **261,** 7123–7126 (1986).
13. Hanna, P. C., Acosta, D. & Collier, R. J. On the role of macrophages in anthrax. *Proc. Natl Acad. Sci. USA* **90,** 10198–10201 (1993).
14. Pellizzari, R., Guidi-Rontani, C., Vitale, G., Mock, M. & Montecucco, C. Anthrax lethal factor cleaves MKK3 in macrophages and inhibits the LPS/IFNγ-induced release of NO and TNFα. *FEBS Lett.* **462,** 199–204 (1999).
15. Ballard, J. D., Collier, R. J. & Starnbach, M. N. Anthrax toxin-mediated delivery of a cytotoxic T-cell epitope *in vivo*. *Proc. Natl Acad. Sci. USA* **93,** 12531–12534 (1996).
16. Goletz, T. J. *et al.* Targeting HIV proteins to the major histocompatibility complex class I processing pathway with a novel gp120–anthrax toxin fusion protein. *Proc. Natl Acad. Sci. USA* **94,** 12059–12064 (1997).
17. Quinn, C. P., Singh, Y., Klimpel, K. R. & Leppla, S. H. Functional mapping of anthrax toxin lethal factor by in-frame insertion mutagenesis. *J. Biol. Chem.* **266,** 20124–20130 (1991).
18. Gupta, P., Singh, A., Chauhun, V. & Bhatnagar, R. Involvement of residues 147VYYEIGK153 in binding of lethal factor to protective antigen of *Bacillus anthracis*. *Biochem. Biophys. Res. Comm.* **280,** 158–163 (2001).
19. Holm, L. & Sander, C. Dali/FSSP classification of three-dimensional protein folds. *Nucleic Acids Res.* **25,** 231–234 (1997).
20. Carroll, S. F. & Collier, R. J. NAD binding site of diphtheria toxin: identification of a residue within the nicotinamide subsite by photochemical modification with NAD. *Proc. Natl Acad. Sci. USA* **81,** 3307–3311 (1984).
21. Mock, W. L. & Stanford, D. L. Arazoformyl dipeptide substrates for thermolysin. Confirmation of a reverse protonation catalytic mechanism. *Biochemistry* **35,** 7369–7377 (1996).
22. Park, S. & Leppla, S. H. Optimized production and purification of *Bacillus anthracis* lethal factor. *Protein Expr. Purif.* **18,** 293–302 (2000).
23. Otwinowski, Z. & Minor, W. Processing of X-ray diffraction data collected in oscillation mode. *Methods Enzymol.* **276,** 307–326 (1997).
24. The CCP4 suite: programs for protein crystallography. *Acta Crystallogr. D* **50,** 760–763 (1994).
25. Terwilliger, T. C. & Berendzen, J. Automated MAD and MIR structure solution. *Acta Crystallogr. D* **55,** 849–861 (1999).
26. Roussel, A. & Cambillau, C. 86 (Silicon Graphics, Mountain View, California, 1991).
27. Brunger, A. T. *et al.* Crystallography & NMR system: A new software suite for macromolecular structure determination. *Acta Crystallogr. D* **54,** 905–921 (1998).
28. Wang, X.-M., Mock, M., Ruysschaert, J.-M. & Cabiaux, V. Secondary structure of anthrax lethal toxin proteins and their interaction with large unilamellar vesicles (LUV): a Fourier-transform infrared spectroscopy approach. *Biochemistry* **35,** 14939–14946 (1996).
29. Bacon, D. J. & Anderson, W. F. A fast algorithm for rendering space-filling molecule pictures. *J. Mol. Graphics* **6,** 219–220 (1988).
30. Kraulis, P. J. Molscript—a program to produce both detailed and schematic plots of protein structures. *J. Appl. Crystallogr.* **24,** 946–950 (1991).
31. Merrit, E. A. & Murphy, M. E. P. Raster3D version 2.0. A program for photorealistic molecular graphics. *Acta Crystallogr. D* **50,** 869–873 (1994).
32. Christopher, J. A. *SPOCK: The Structural Properties Observation and Calculation Kit (Program Manual)* (The Center for Macromolecular Design, Texas A&M University, College Station, 1998).

Supplementary information is available on *Nature*'s World-Wide Web site (http://www.nature.com) or as paper copy from the London editorial office of *Nature*.

Acknowledgements

We thank L. Bankston for discussion and D. Hsu for LF preparations. We thank and acknowledge the staff and facilities of the synchrotron sources at SSRL, Stanford; SRS, Daresbury; ESRF, Grenoble; APS, Chicago; and National Synchrotron Light Source, Brookhaven. Supported by grants from the Medical Research Council and the National Institutes of Health.

Correspondence and requests for materials should be addressed to R.C.L (e-mail: rlidding@burnham.org). Coordinates for the monoclinic LF crystal structure and the cubic LF–MAPKK2 complex have been deposited with the Protein Data Bank (accession codes 1J7N and 1JKY, respectively).